Check for updates

NANO · MICRO small
www.small-journal.com

Size-Dependent Locomotion Ability of Surface Microrollers on Physiologically Relevant Microtopographical Surfaces

*Ugur Bozuyuk, Erdost Yildiz, Mertcan Han, Sinan Ozgun Demir, and Metin Sitti**

Controlled microrobotic navigation inside the body possesses significant potential for various biomedical engineering applications. Successful application requires considering imaging, control, and biocompatibility. Interaction with biological environments is also a crucial factor in ensuring safe application, but can also pose counterintuitive hydrodynamic barriers, limiting the use of microrobots. Surface rolling microrobots or surface microrollers is a robust microrobotic platform with significant potential for various applications; however, conventional spherical microrollers have limited locomotion ability over biological surfaces due to microtopography effects resulting from cell microtopography in the size range of 2–5 µm. Here, the impact of the microtopography effect on spherical microrollers of different sizes (5, 10, 25, and 50 µm) is investigated using computational fluid dynamics simulations and experiments. Simulations revealed that the microtopography effect becomes insignificant for increasing microroller sizes, such as 50 µm. Moreover, it is demonstrated that 50 µm microrollers exhibited smooth locomotion ability on in vitro cell layers and inside blood vessels of a chicken embryo model. These findings offer rational design principles for surface microrollers for their potential practical biomedical applications.

1. Introduction

Mobile microrobots were promised as next-generation drug/gene delivery agents owing to their active propulsion and steerability[1] to access hard-to-reach regions in the body. Even though microrobotic research in the past decade mainly focused on exploring novel actuation and control schemes,[2] drug release,[3] biocompatibility,[4] and imaging,[4b,5] the interaction between microrobots and biological environments was often overlooked, which also created unprecedented hydrodynamic barriers for their locomotion.[6]

Magnetically actuated surface rolling microrobots, i.e., surface microrollers, is a practical microrobotic platform that has been shown to produce strong propulsion and navigate in physiologically relevant flows.[4b,6a,7] Other than important considerations of microrollers for their applications in the human body, such as biocompatibility and imaging,[4b] their hydrodynamic interactions with their surrounding media were also shown to render additional barriers to their use.[6,8] For example, the texture of the nearby wall has been shown to have a significant impact on the locomotion of surface microrollers, impeding their locomotion due to counterintuitive hydrodynamic effects.[6a] In our recent work, we demonstrated that surface microtopography caused by biological cells of 2–3 µm height created a significant hydrodynamic locomotion barrier for conventional 8 µm spherical microrollers.[6a] To perform tasks on biologically relevant media, microrobots need to exhibit robust locomotion on such textured surfaces.

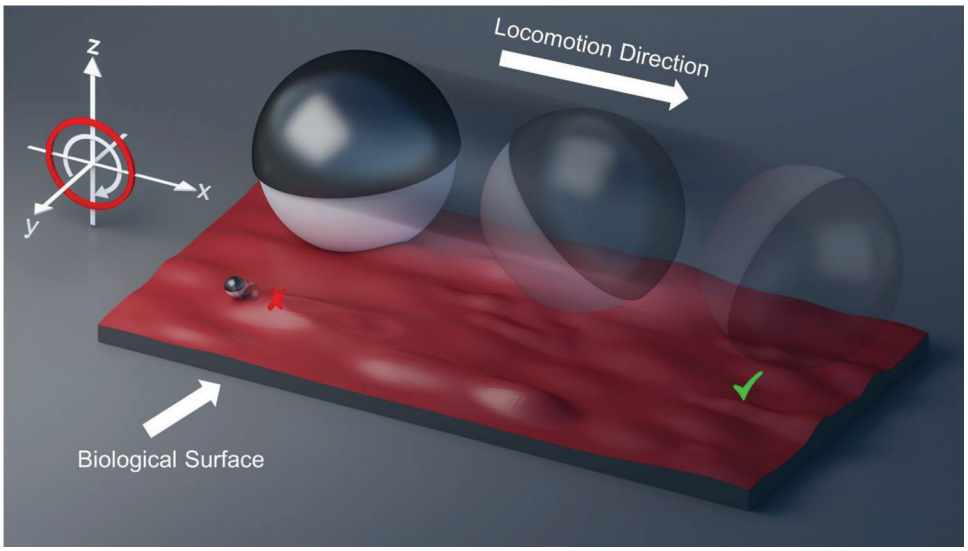
Here, we explored the size-dependent locomotion ability of spherical surface microrollers with diameters of 5, 10, 25, and 50 µm near microtopographies in computational fluid dynamics (CFD) analyses. We simulated microrollers near biologically relevant-sized microtopographies and predicted their locomotion ability. The quantitative results demonstrated that the microtopography effect became less significant as the microroller diameter increased; the surface behaved like a roughness rather than a microtopographic for bigger microrollers (**Scheme 1**). Furthermore, we experimentally demonstrated the unimpeded locomotion ability of 50 µm microroller over in vitro cells and blood vessels of the chicken embryo model, validating the findings in CFD simulations. Our findings provide insight for the rational design of surface microrollers to reduce hydrodynamic barriers in their future in vivo applications.

U. Bozuyuk, E. Yildiz, M. Han, S. O. Demir, M. Sitti
Physical Intelligence Department
Max Planck Institute for Intelligent Systems
70569 Stuttgart, Germany
E-mail: sitti@is.mpg.de
U. Bozuyuk, M. Han, M. Sitti
Institute for Biomedical Engineering
ETH Zurich
Zurich 8092, Switzerland
M. Sitti
School of Medicine and School of Engineering
Koç University
Istanbul 34450, Turkey

The ORCID identification number(s) for the author(s) of this article can be found under https://doi.org/10.1002/smll.202303396

© 2023 The Authors. Small published by Wiley-VCH GmbH. This is an open access article under the terms of the Creative Commons Attribution License, which permits use, distribution and reproduction in any medium, provided the original work is properly cited.

DOI: 10.1002/smll.202303396



Scheme 1. Magnetic microrollers on biological surfaces. The small microroller is unable to perform translational locomotion on biological surfaces due to hydrodynamic barriers resulting from the microtopography of the biological cells. In contrast, the larger microroller is unaffected by the microtopography effect, enabling it to perform translational locomotion smoothly.

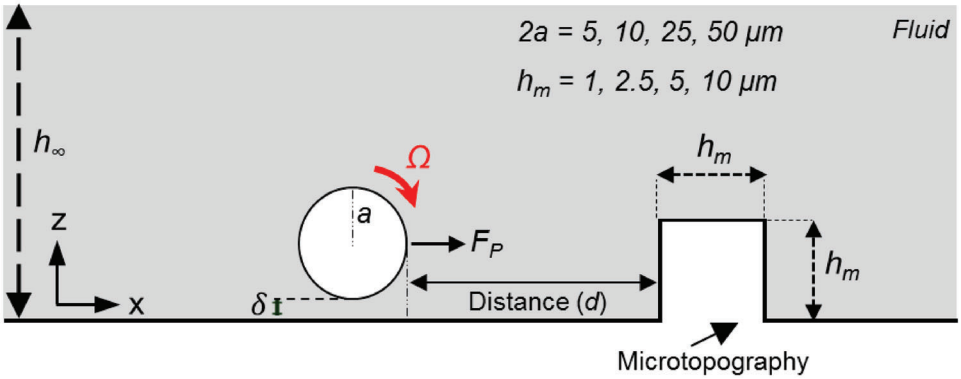
2. Results

2.1. Computational Fluid Dynamics Analyses Near Microtopographies

We characterized the locomotion ability of different sizes of microrollers, 5, 10, 25, and 50 µm diameter in the vicinity of simplified, rectangular microtopographies with fixed dimensions (**Scheme 2**) with previously developed and validated 3D CFD analyses.[6b] The microtopography sizes were selected as $h_m = 1$, 2.5, 5, and 10 µm, representing the cell microtopographies found in the human body, such as the inner wall of blood vessels[9] and epithelial cells,[10] while $h_m = 10$ µm is an exaggerated example. The fixed microrollers were rotated with $f = 100$ Hz for increasing lubrication distances ($\delta' = \delta/a$), the distance between the microroller and nearby wall (Scheme 2), where they were gradually approached the microtopographies with a distance of (d). The hydrodynamic forces acting on the spheres were quantified in each case according to:

$$F = \iint \boldsymbol{\sigma} \times \boldsymbol{n}\, \mathrm{d}S \tag{1}$$

where σ is the stress tensor, n is the outward pointing normal vector, and S is the particle surface. The total acting force resulted in $+x$ direction with clockwise rotation of the body, which is propulsion force, F_P, generated by the microroller (Scheme 2) that determines the microroller's translational speed (V).[6,7,11] We calculated the relative F_P decreases compared to the F_P value in a semi-infinite and topography-free environment for each case. Overall, the relative F_P drops gave information about the locomotion capability of microrollers near the microtopographies; >100% F_P decrease indicated the backward, thus hindered locomotion. Throughout the manuscript, the results were



Scheme 2. The summary of the CFD simulations. Microrollers placed in a semi-infinite rectangular channel in 3D. A microtopography with dimensions of $h_m \times y \times h_m$ was placed at the bottom of the channel. Microrollers having 2a diameter with an angular velocity of omega was approached to the microtopography for different lubrication distances, $\delta' = \delta/a$. The forces, F_P, generated by microrollers were quantified and compared to forces without microtopography in the semi-infinite media.

 © 2023 The Authors. Small published by Wiley-VCH GmbH

16136829, 2023, 47, Downloaded from https://onlinelibrary.wiley.com/doi/10.1002/smll.202303396 by Turkey Cochrane Evidence Aid, Wiley Online Library on [30/02/2025]. See the Terms and Conditions (https://onlinelibrary.wiley.com/terms-and-conditions) on Wiley Online Library for rules of use; OA articles are governed by the applicable Creative Commons License

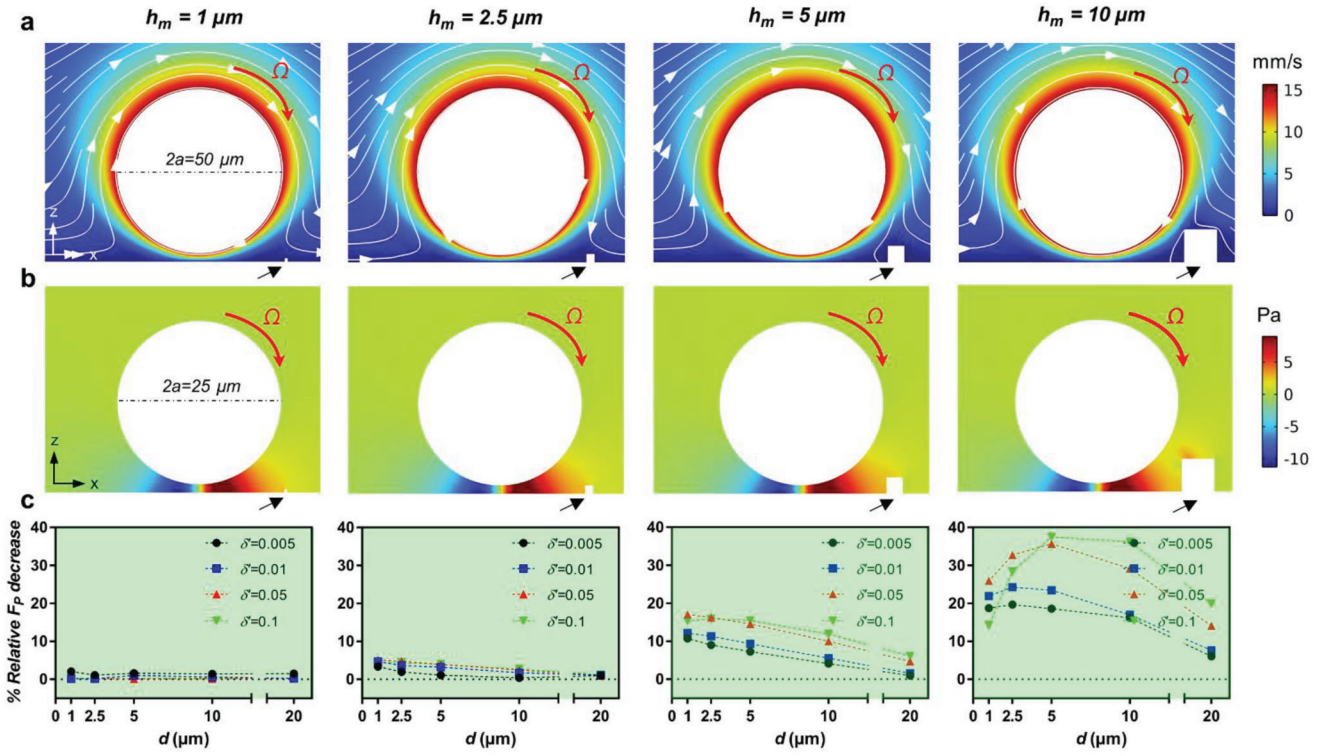


Figure 1. The CFD analyses for 2a = 50 μm microroller near microtopographies. a) Cross-sectional images of the flow fields and b) pressure distribution around the microrollers near (d = 1 μm) different microtopographies at δ'= 0.1. Microtopographies were pointed with black arrows. c) The propulsion force decrease against different distances from the topography for different δ' values, higher δ' implying higher actuation frequencies. The microroller can perform forward locomotion at any condition since the relative propulsion force decrease was not >100%, highlighted by the green color in the graph.

represented by d versus % relative F_P decrease for different δ', where relatively lower and higher δ' indicated the smaller and higher rotation frequency, f, region, respectively.[6b] The δ' in reality is deterministically reached to a value depending on the f. It must be noted that the relative F_P decreases will be the same at any f value for fixed δ' due to the linearity of the system for f.[6b,11] In other words, f is not a critical parameter while calculating the relative F_P decreases in the CFD environment, rather $\delta'$is critical since it expresses the increase of f.[6b,12] Therefore, relatively smaller δ' values represent smaller f and vice versa.

The relative size of the 50 μm microroller is higher compared to microtopographies studied here, h_m = 1, 2.5, 5, and 10 μm (**Figure 1**a,b); therefore, one would expect smooth locomotion on such microtopographies. From the first qualitative impression, the hydrodynamic flowfields around the microrollers were relatively unaffected near the microtopographies, except h_m = 10 μm (Figure 1a). The forces acting on the microrollers comprise of viscous and pressure terms, and our previous work demonstrated that the pressure forces started to increase and dominate near the microtopographies.[6a] Therefore, the qualitative pressure field analyses have also shown no prominent pressure generation near the microtopographies with the closest distance, d = 1 μm, except h_m = 10 μm, implying the microroller was not pushed by the microtopographies (Figure 1b). The quantitative results indeed supported the abovementioned statements, the relative force decreases for h_m = 1 μm almost negligible for any d and δ' (Figure 1c). On the other hand, the extent of the % relative F_P decreases increased with larger topography sizes and reached almost 20% for d = 1 μm, h_m = 5 μm and δ' = 0.1 (Figure 1c). The previous study has shown that the microroller locomotion near the microtopographies was unsuccessful when the f is relatively high, even though the microrollers have higher translational speed in non-topographic media.[6a] A similar trend is also observed in the simulations; the higher δ' values usually had more force drops except when microrollers were very close to the microtopography (e.g., h_m = 5 μm, d = 5, 10, and 20 μm in Figure 1c). However, this trend seemed to transform near the microtopography (e.g., d = 1 μm), especially in bigger microtopography sizes. For example, for h_m = 5 μm, d = 1 μm, the relative force decrease for δ' = 0.1 became smaller than δ' = 0.05. This trend was more prominent for h_m = 10 μm. The force decrease first reached a peak value for all δ' while the microroller was approaching the microtopography, and then suddenly dropped when the microroller was very near to the microtopography (Figure 1c). When the microroller was very close to the microtopography, d = 1, the higher frequency region (i.e., higher δ'), had the lowest decrease and could locomote over the microtopography. On the other hand, if the relative force (%) decrease exceeds 100% before the microroller gets near the microtopography, it would be hydrodynamically trapped before the microtopography and rotate without translation.[6a] Overall, the results for 50 μm microroller have suggested that it could perform smooth locomotion on microtopographic surfaces since the relative force decreases did not exceed >100%; in fact, the highest drop was 40% (d = 5 μm,

 © 2023 The Authors. Small published by Wiley-VCH GmbH

16136829, 2023, 47, Downloaded from https://onlinelibrary.wiley.com/doi/10.1002/smll.202303396 by Turkey Cochrane Evidence Aid, Wiley Online Library on [20/02/2025]. See the Terms and Conditions (https://onlinelibrary.wiley.com/terms-and-conditions) on Wiley Online Library for rules of use; OA articles are governed by the applicable Creative Commons License

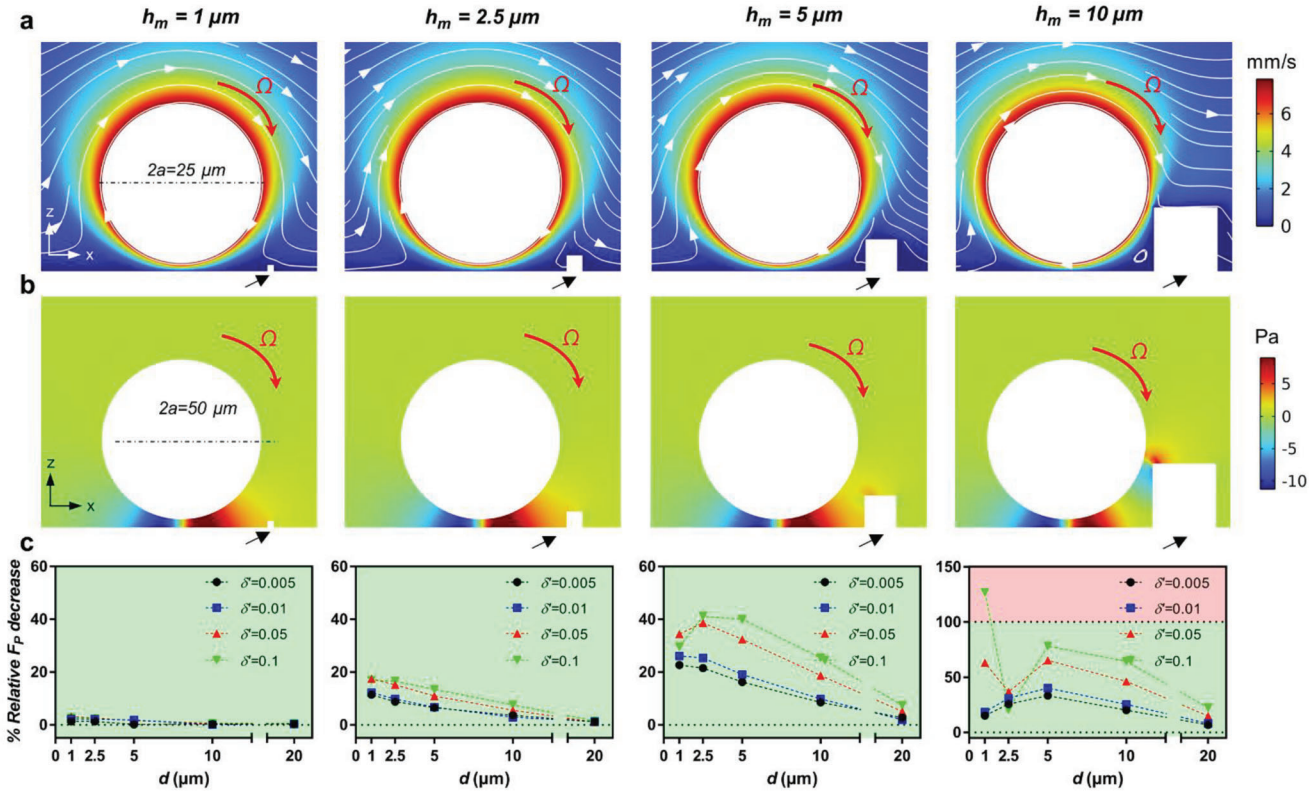


Figure 2. The CFD analyses for 2a = 25 μm microroller near microtopographies. a) The flow fields and b) pressure distribution around the microrollers near (d = 1 μm) different microtopographies at δ' = 0.1. c) The propulsion force decrease against different distances from the topography for different δ' values. The green and red regions indicate forward and backward locomotion, respectively. The red region implies that the microrollers are propelled by the microtopography. The 25 μm microroller could no longer perform forward locomotion near the biggest topography, h_m = 10 at d = 1, for higher actuation frequencies/increased delta, highlighted by the red region.

δ' = 0.1, Figure 1c). The microtopography sizes studied here acted more like a surface roughness for 50 μm microroller; thus, the locomotion is estimated to be unimpeded for biologically relevant microtopographies with the sizes h_m = 1, 2.5, and 5 μm.

25 μm microroller followed a similar pattern as the 50 μm one, where the flowfields seemed undisturbed for all microtopographies except h_m = 10 μm due to increased microtopography/microroller ratio (**Figure 2**a). The qualitative pressure field analyses have shown the pressure accumulation near the boundary between the microroller and microtopography for the d = 10 μm, δ' = 0.1, implying that the microroller could be pushed by the wall (Figure 2b). The force quantifications have demonstrated that the relative force decreases were almost insignificant for h_m = 1 and 2.5 μm (Figure 2c). A similar trend was observed for h_m = 5 μm (Figure 2c) as previously shown for 50 μm microroller for h_m = 10 μm (Figure 1c). Still, the relative force drops were way below 100%. For h_m = 10 μm, an interesting behavior was observed for the relatively higher δ' values such as δ' = 0.05 and 0.1; first, the force reductions increased while the microroller was approaching the microtopography and then started to drop as also previously shown (h_m = 10 μm, Figure 1c). However, then force drops suddenly increased at d = 1 μm and exceed 100% for δ' = 0.1, implying that the wall would push the microroller (Figure 2c). Therefore, the results propose that the locomotion performance of 25 μm microroller seems robust for topographies of h_m = 1, 2.5, and 5 μm but may be problematic for h_m = 10 μm, especially at higher f region.

The microtopography/microroller ratio increases for 10 μm microroller; therefore, the relative force decreases were expected to be higher. The hydrodynamic flow fields were diverted due to the presence of the microtopographies, especially for h_m = 5 and 10 μm (**Figure 3**a). In addition, similar to the 25 μm, the pressure accumulation between the microroller and the microtopography was noticed (Figure 3b). The force analyses revealed that even h_m = 1 μm microtopography affected the performance of 10 μm microroller, reaching ≈25% force decrease for high f region, δ' = 0.1 (Figure 3c). Interestingly, the force decrease was almost 100% for h_m = 5 μm and δ' = 0.1 at d = 2.5 μm, but then became almost 0% when the microroller was closer to the microtopography, d = 1 μm (Figure 3c). At the microtopography of h_m = 10 μm size, the 10 μm microroller failed in the high f region, at δ' = 0.05 and 0.1. The 10 μm microroller, in general, could perform successful locomotion in h_m = 1 and 2.5 μm microtopographies, and the larger sizes could be problematic, especially at high f regions.

The smallest microroller studied here, 5 μm in diameter, was expected to be the worst-performing microroller due to the increased microtopography/microroller ratio. The hydrodynamic flow fields were affected by the microtopography almost for all microtopography other than h_m = 1 μm (**Figure 4**a). On the other hand, qualitatively, a pressure accumulation between microroller

© 2023 The Authors. Small published by Wiley-VCH GmbH

16136829, 2023, 47, Downloaded from https://onlinelibrary.wiley.com/doi/10.1002/smll.202303396 by Turkey Cochrane Evidence Aid, Wiley Online Library on [20/02/2025]. See the Terms and Conditions (https://onlinelibrary.wiley.com/terms-and-conditions) on Wiley Online Library for rules of use; OA articles are governed by the applicable Creative Commons License

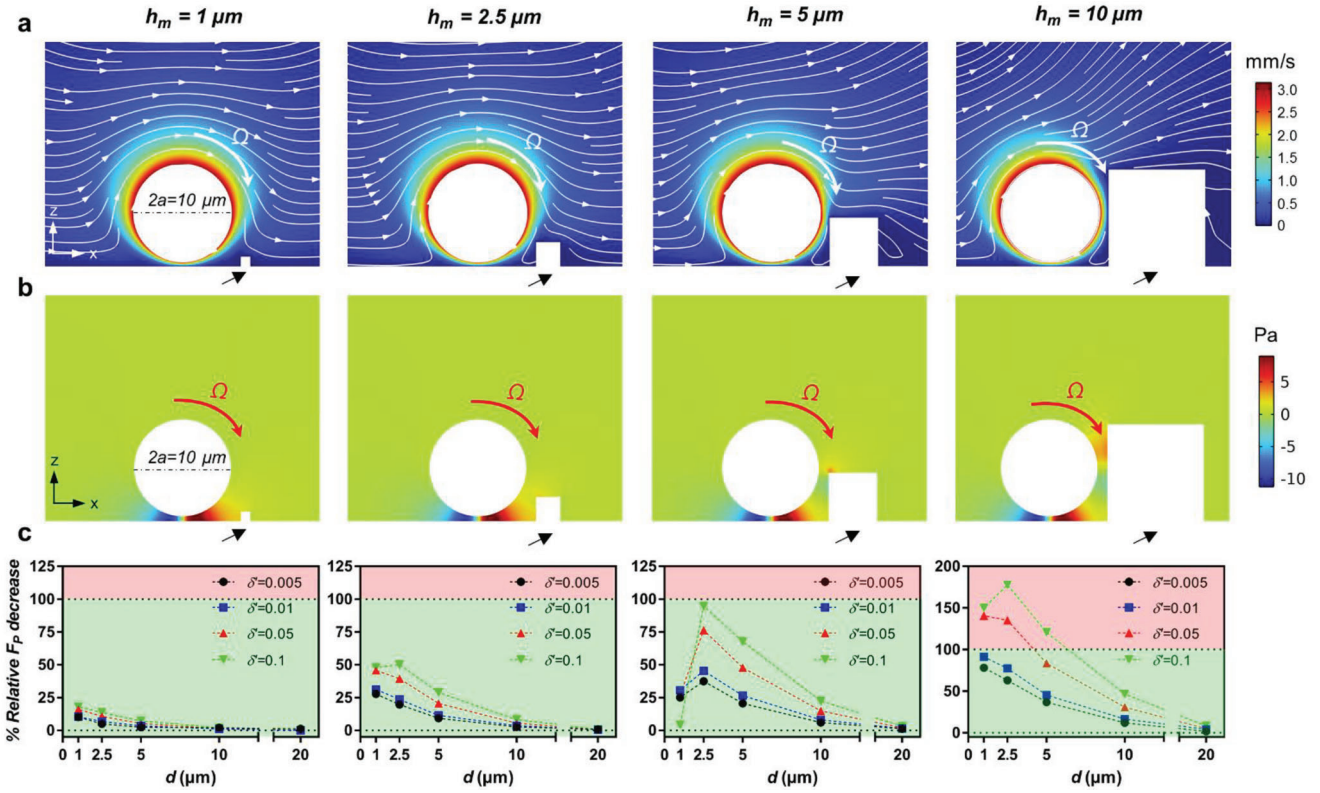


Figure 3. The CFD analyses for 2a = 10 μm microroller near microtopographies. a) The flow fields and b) pressure distribution around the microrollers near (d = 1 μm) different microtopographies at δ' = 0.1. c) The universal propulsion force decrease against different distances from the topography for different δ' values. The green and red regions indicate forward and backward locomotion, respectively. The red region implies that the microrollers are propelled by the microtopography. The 10 μm microroller tends to fail locomoting over microtopographies due to decreased microroller/topography ratio.

and microtopography was not observed for the closest distance d = 1 μm (Figure 4b), probably due to microroller's relative distance to the microtopography was not sufficiently close. The force analyses for the 5 μm revealed that the locomotion of such microroller would be challenging in microtopographic media except for h_m = 1 μm, still, 50% force drop was noticed for d = 1 μm at δ' = 0.1. Overall, the results presented in this study demonstrated that the bigger microroller sizes are advantageous on biologically relevant microtopography sizes. After a certain threshold of microroller diameter, the biologically relevant surfaces probably act as roughness rather than microtopographic. For smaller microrollers, increased actuation frequency, or δ', created more significant force reductions near the microtopographies, as previously experimentally characterized.[6a] The irregular force drops were also observed when microrollers were very near to microtopography. In addition, the locomotion barrier of 5 μm near microtopographies could be partially tackled with swarming microrollers. To study the effect of swarming microrollers, we modeled 5 μm microrollers next to each other, at which the nearest microrollers had d = 1 μm distance from topographies with h_m = 1, 2.5, 5, and 10 μm (Figure S1, Supporting Information). When three swarming microrollers to close each other in the swarm at the distance of 0.5 μm, the front microroller performed forward locomotion near the microtopography of h_m = 5 μm at high δ' region, while the single microroller was pushed by the wall to the reverse direction (Figure S1a–d, Supporting Information). This effect slightly increased for five swarming microrollers, again especially at a high δ'region (Figure S1e,f, Supporting Information). Overall, the swarm simulations suggested that the swarming effect could be beneficial for small microrollers to overcome microtopographies.

2.2. Microrollers on Synthetic Microtopographies

We have demonstrated the locomotion performance of microrollers on synthetic microtopographies with h_m = 1, 2.5, 5, and 10 μm, similar to the simulation environment (**Figure 5**a). The 5 and 50 μm microrollers were fabricated using silica microparticles half coated with Ni and Au magnetic film, while Au prevents oxidation of Ni, which was previously characterized.[13] The 5 μm contained 1000 nm Ni and 50 nm Au, and the 50 μm microroller 1800 nm Ni and 50 nm Au respectively. Silica is a well-established bio-friendly and practical material,[14] and a wide range of sizes are commercially available in a cost-friendly manner. Therefore, silica microparticles with different sizes easily allowed us to study different dynamics of the system. On the other hand, while Ni is known to be an allergenic and toxic material,[15] it is still a practical option for deposition using simple sputtering devices. Due to its practicality,

© 2023 The Authors. Small published by Wiley-VCH GmbH

16136829, 2023, 47, Downloaded from https://onlinelibrary.wiley.com/doi/10.1002/smll.202303396 by Turkey Cochrane Evidence Aid, Wiley Online Library on [20/02/2025]. See the Terms and Conditions (https://onlinelibrary.wiley.com/terms-and-conditions) on Wiley Online Library for rules of use; OA articles are governed by the applicable Creative Commons License

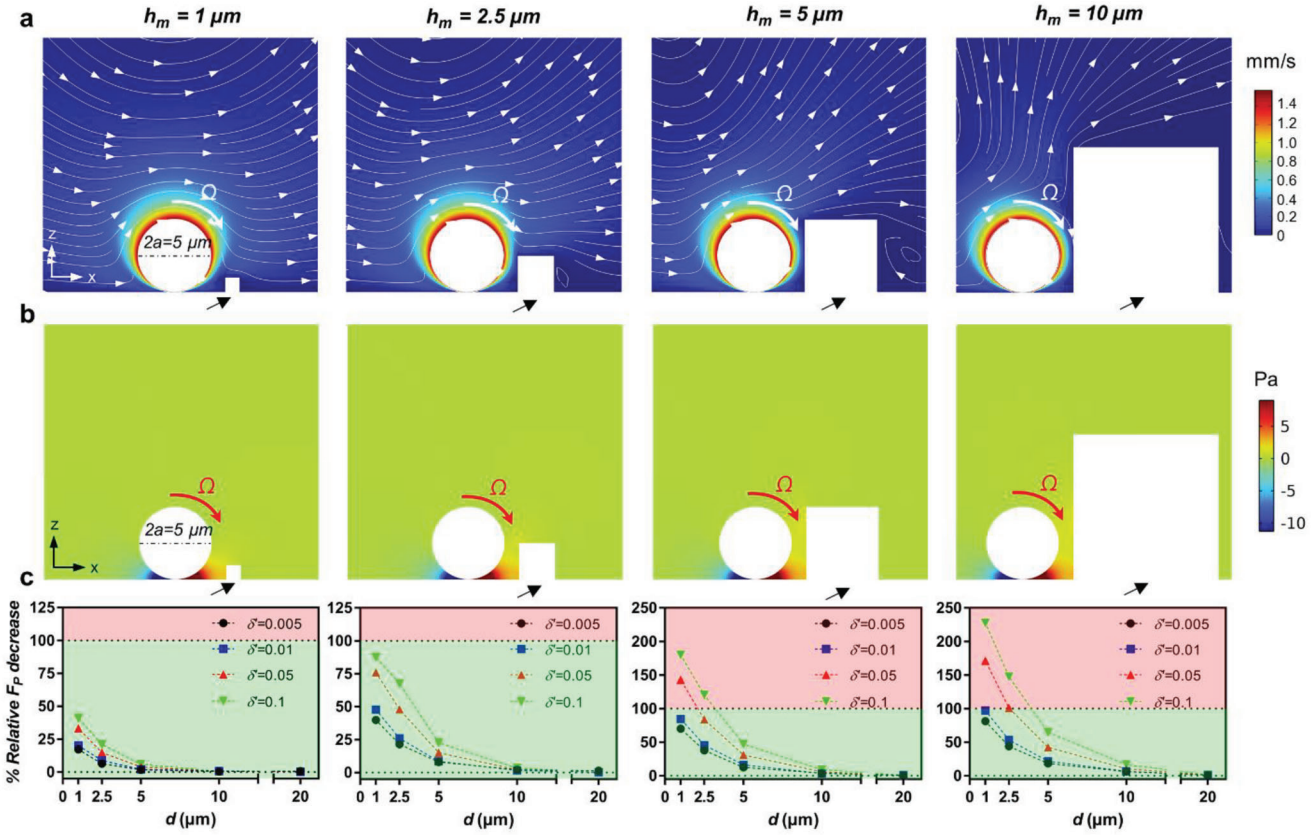


Figure 4. The CFD analyses for 2a = 5 μm microroller near microtopographies. a) The flow fields and b) pressure distribution around the microrollers near (d = 1 μm) different microtopographies at $\delta' = 0.1$. c) The universal propulsion force decreases against different distances from the topography for different delta values. The green and red regions indicate forward and backward locomotion, respectively. The red region implies that the microrollers are propelled by the microtopography. As expected, the 5 μm microroller had the worst performance in forward locomotion due to decreased microroller/microtopography ratio.

wafer-scale particles can be prepared in less than an overnight process. However, it is not suitable for real biomedical applications, as we have demonstrated in our previous study. Still, they can be easily replaced by their biocompatible counterparts, such as $L1_0$-FePt.[4b] Overall, the materials used in this study enabled us to investigate the physical characteristics of microrollers robustly, thanks to their practicality. However, these materials can be substituted with more complex and advantageous alternatives for the biomedical applications of microrollers.

We microfabricated synthetic microtopographies with two-photon lithography and locomoted 5 and 50 μm microrollers on these topographies with 10 and 80 Hz actuation frequency,[13] representing low and high δ' regions in the simulations, respectively (Figure 5a). The results are summarized in Figure 5b. At the low actuation frequency, f = 10 Hz, the 5 μm microrollers were able to successfully locomote over the microtopographies of h_m = 1, 2.5, 5 μm, but failed against h_m = 10 μm (Figure 5b,c; Movie S1, Supporting Information). When the actuated frequency was increased to f = 80 Hz, it started to fail to locomote even in smaller topographies, similar to our previous work (Figure 5b,d; Movie S1, Supporting Information).[6a] Namely, they performed rotational locomotion without translational motion near the microtopographies due to the flow field generated around the microroller, and the microtopography pushed them.[6a] Conversely, 50 μm microroller performed successful locomotion on any synthetic microtopography for both actuation frequencies (Figure 5b,e,f; Movie S1, Supporting Information), further validating the simulation results.

2.3. Microrollers on Biological Microtopographies

This section shows two brief experimental demonstrations of microrollers on biological topographies. In the first one, we compared the performance of 5 and 50 μm microrollers on highly packed HT-29 colon epithelial cells (**Figure 6**a). The HT-29 cells presented 2–3 μm sized microtopography height due to their cell nuclei, which was characterized in our previous study.[16] The organization of the packed cells was not ordered, meaning that the topography organization was also complex in three dimensions.

The magnetic microrollers were actuated with out-of-plane uniform rotating magnetic fields to break the hydrodynamic flowfield symmetry and obtain rolling locomotion (Figure 6a). We

© 2023 The Authors. Small published by Wiley-VCH GmbH

16136829, 2023, 47, Downloaded from https://onlinelibrary.wiley.com/doi/10.1002/smll.202303396 by Turkey Cochrane Evidence Aid, Wiley Online Library on [20/02/2025]. See the Terms and Conditions (https://onlinelibrary.wiley.com/terms-and-conditions) on Wiley Online Library for rules of use; OA articles are governed by the applicable Creative Commons License

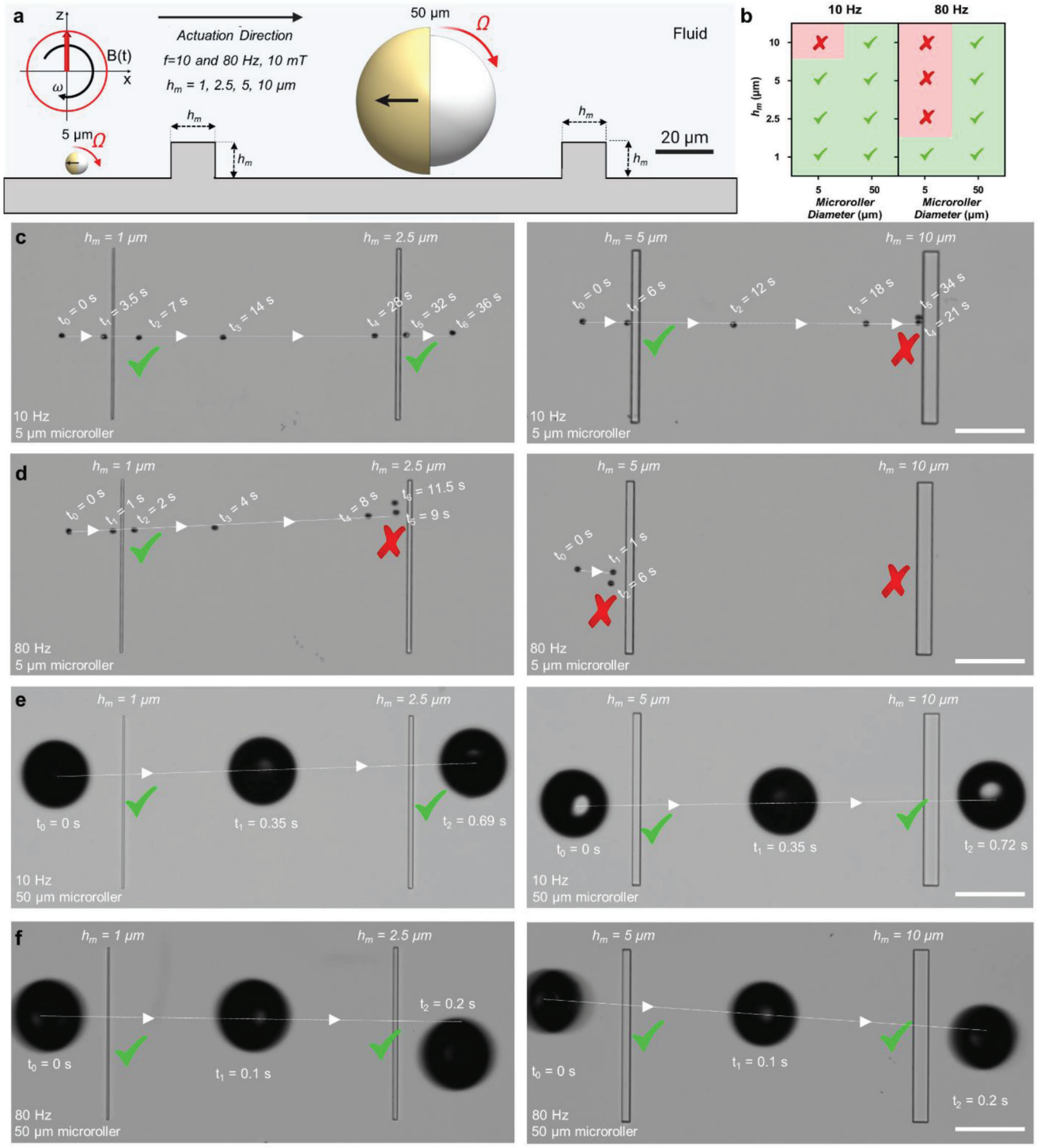


Figure 5. The microroller locomotion over synthetic microtopographies. a) The summary of the experiments. The 5 and 50 μm microrollers were driven over the synthetic microtopographies similar to the simulation environment with the h_m = 1, 2.5, 5, and 10 μm with $f = \Omega/2a$ = 10 and 80 Hz. b) The performance diagram of microrollers over synthetic microtopographies. As predicted in CFD analyses, 5 μm microroller was less successful than 50 μm. c,d) Time-lapse images of 5 μm microroller with f = 10 and 80 Hz, over synthetic microtopographies. At f = 10 Hz, the microroller locomoted over the h_m = 1, 2.5, and 5 μm, but failed at h_m = 10 μm. On the other hand, f = 80 Hz, the microroller failed even at h_m = 2.5 μm. In addition, it also failed at h_m = 5 and 10 μm, as expected (Movie S1, Supporting Information). e,f) Time-lapse images of 50 μm microroller with f = 10 and 80 Hz, over synthetic microtopographies. The microroller could locomote over all microtopographies as predicted in CFD analyses.

© 2023 The Authors. Small published by Wiley-VCH GmbH

16136829, 2023, 47, Downloaded from https://onlinelibrary.wiley.com/doi/10.1002/smll.202303396 by Turkey Cochrane Evidence Aid, Wiley Online Library on [20/02/2025]. See the Terms and Conditions (https://onlinelibrary.wiley.com/terms-and-conditions) on Wiley Online Library for rules of use; OA articles are governed by the applicable Creative Commons License

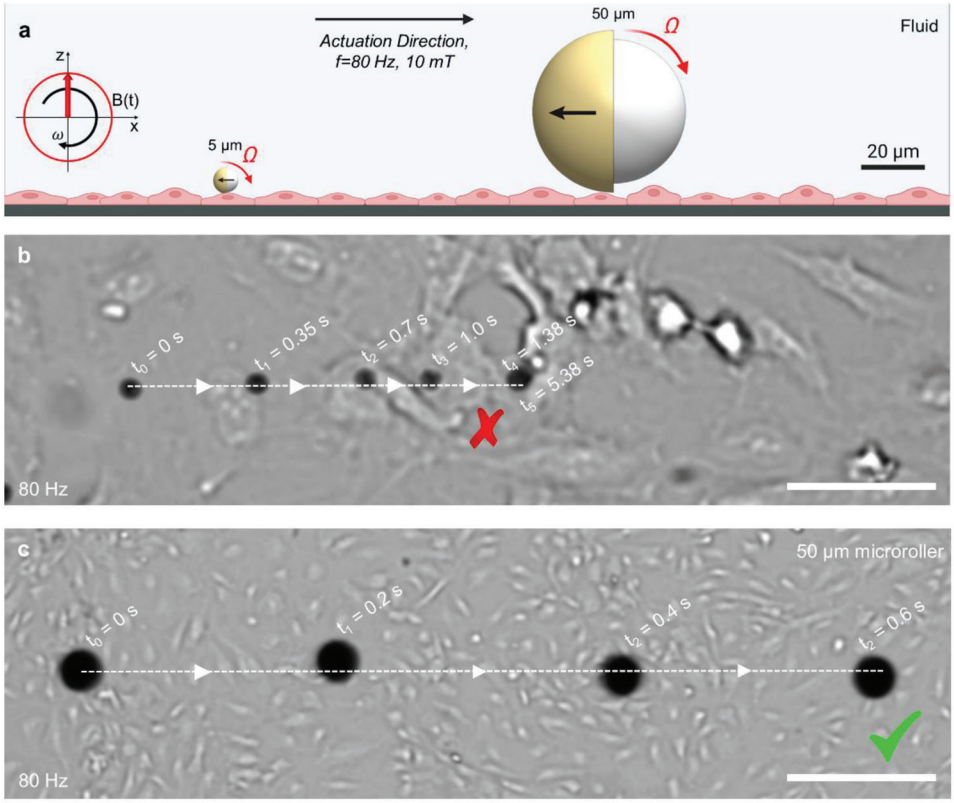


Figure 6. The microroller locomotion over in vitro cultured cell layers. a) The summary of the experiments. Microrollers of 5 and 50 μm were actuated on the cells from left to right with $f = \Omega/2a = 80$ Hz, on HT-29 cell line presenting 2–4 um micrometer microtopographies.[16] Scale bar: 20 μm. b) The 5 μm microroller failed to perform on the cell layers. After $t_4 = 1.38$, the microroller could not perform translational locomotion despite constant rotation. Scale bar: 50 μm. c) Conversely, the 50 μm microroller performed smooth translational locomotion due to decreased microtopography effect in that scale. Scale bar: 200 μm.

actuated the microrollers at 80 Hz, which was the step-out frequency for 50 μm microroller, while 5 μm was not also stepped-out at 80 Hz.[13] It is well-known that microrobots with higher speeds are usually desirable to overcome external fluidic flows in the body. Therefore, we performed the in vitro demonstration with the highest actuation frequency, 80 Hz. When 5 μm actuated on the cells, it was first able to locomote but then hydrodynamically trapped near the microtopography (Figure 6b; Movie S2, Supporting Information). Even though it was constantly rotating, the microroller was not able to perform translational locomotion as the CFD simulations previously suggested for 5 μm (Figure 4b). On the other hand, 50 μm microroller locomoted on the cells as if there were no cells underneath (Figure 6c; Movie S2, Supporting Information). The locomotion was smooth and fast, probably due to the microtopographies acting like roughness on the surface due to the high microroller/microtopography ratio. Overall, the first experimental demonstration supported the findings in CFD simulations; it was previously predicted that the locomotion would be smoother with 50 μm since forces generated by the microrollers were hardly affected by the presence of microtopographies. Still, the locomotion trajectories of the microrollers were not fully smooth due to the presence of microtopographies (Figure 6b,c), unlike the locomotion on glass substrates.[6,7] Ideally, more accurate trajectories could be obtained by deploying close-loop imaging feedback control systems, which require rigorous investigation.

The second experimental demonstration included the locomotion of 50 μm microroller in the blood vessels of the chicken embryo model. We selected 50 μm microrollers for such a demonstration since the previous CFD results and in vitro demonstrations suggested that it would render the safest locomotion on microtopographic surfaces. Additionally, we previously showed that the 50 μm microroller was the more efficient microroller in terms of body length/second compared to 5, 10, and 25 μm microrollers owing to its decreased lubrication distance in our previous work.[13] To perform locomotion in blood vessels, we incubated fertilized White Leghorn chicken eggs up to Hamburger and Hamilton (HH) embryonic stage 36, until they had relevant physiological blood circulation (**Figure 7**a).[17] In HH stage 36, having confirmed the vessel formation and physiological circulation via stereomicroscope (Movie S3, Supporting Information), we injected microrollers into the blood vessels of the chicken embryo with the help of a micropipette (Figure 7b, Supporting Information). It should be noted that the injection of microrollers into the vessel of the chicken embryo was highly challenging due to the following reasons: 1) The injection of microparticles is generally challenging due to dispersion problems in the needle. The efficiency of the injections is usually very low compared to the conventional molecule- or nanoparticle-based systems,[18] which

 © 2023 The Authors. Small published by Wiley-VCH GmbH

16136829, 2023, 47, Downloaded from https://onlinelibrary.wiley.com/doi/10.1002/smll.202303396 by Turkey Cochrane Evidence Aid, Wiley Online Library on [20/02/2025]. See the Terms and Conditions (https://onlinelibrary.wiley.com/terms-and-conditions) on Wiley Online Library for rules of use; OA articles are governed by the applicable Creative Commons License

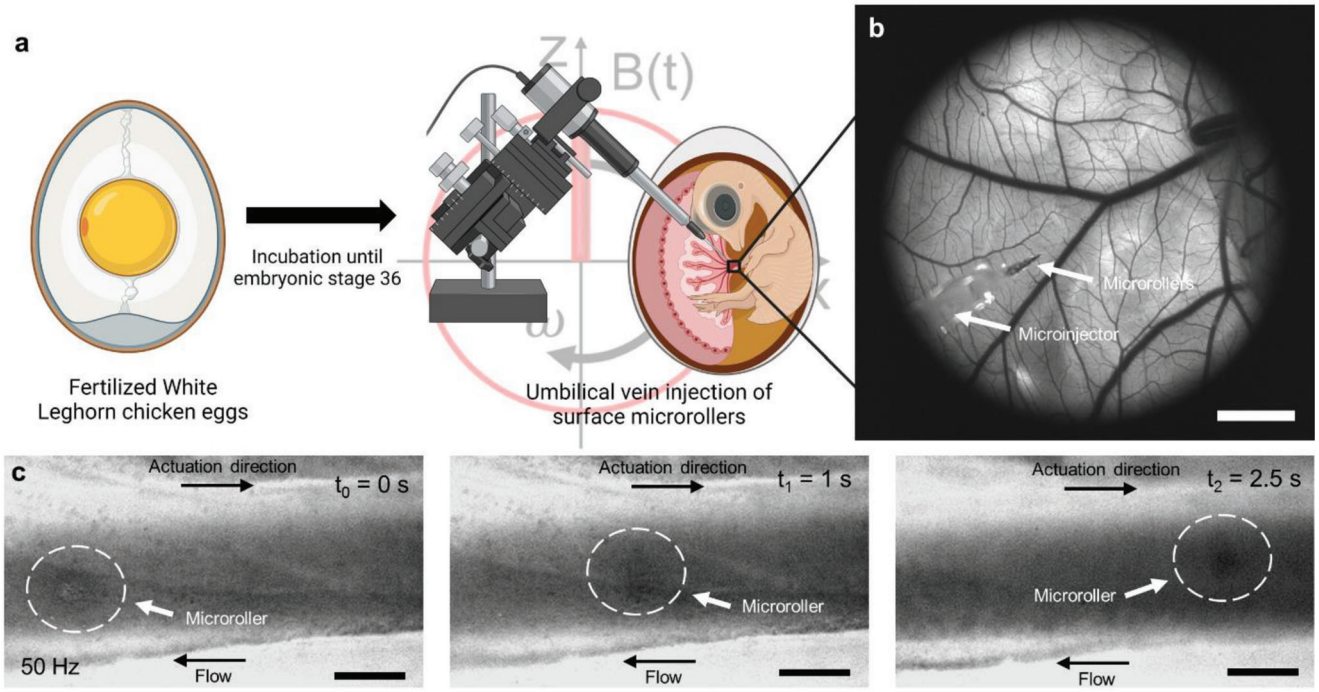


Figure 7. Locomotion of 50 µm microrollers in a chicken embryo model. a) The summary of experimental procedures. The fertilized White Leghorn chicken eggs were incubated until they have physiologically relevant blood flows. In Hamburger–Hamilton stage 36, the chicken embryo was placed in a custom-made coil system under a stereomicroscope, and microrollers were injected with a microinjector. b) A representative image of blood vessels of the chicken embryo and microinjector filled with microrollers. Scale bar: 3 mm. c) A time-lapse image of a 50 µm microroller, performing upstream locomotion in a blood vessel. Scale bar: 100 µm. The average translational velocity of microroller is 179 µm s^{-1}.

was eventually the case for the microrollers. However, this problem can be tackled by developing relatively complex algorithms for injections.[19] 2) The top of the blood vessels was covered with an elastic membrane, which created a significant complexity during the injection and ideally needed to be removed with microsurgery tools by an expert. 3) The tip of the microinjector needs to be custom prepared,sharpened, and beveled to achieve a safe rupturing of the vessel, which needs optimization depending on the nature of the vessel. 4) An appropriate micromanipulator with a proper puncturing force is needed to achieve a safe injection. Overall, the injection of microrollers was challenging due to the abovementioned issues, and the injection system must be improved to achieve more successful injections. Nevertheless, we were able to inject and observe a microroller in the blood vessels of the chicken embryo in a custom-made coil system under a stereo microscope (Figures S2 and S3, Supporting Information). Upon injection, we spotted a single 50 µm microroller and actuated it against the blood flow. The microroller was able to perform upstream locomotion, further proving that the spherical microroller with the appropriate size had no problem actuating on physiological topographies (Figure 7c; Movie S3, Supporting Information).

Other than locomotion considerations, the movement of microrollers on biological cells can potentially lead to negative consequences because of the forces applied to the cells. As a microroller moves, it generates a propulsive force in the direction of its movement and exerts a gravitational force on the surface it rolls on (Note S1 and Figure S4, Supporting Information).[6,7] The order of these forces in a few nN levels, while rupture of cell membranes requires tens of kPa stresses (Note S1 and Figure S5, Supporting Information).[20] With an exaggerated assumption of contact, the area is 1 μm^2, which would be much higher in a real case, the momentary stress applied by the microroller would be ≈1 kPa. Therefore, it is reasonable to infer that the locomotion of microrollers on biological cells may be entirely safe. Another factor to consider is that these forces are applied for a brief duration since the microrollers have a high translational speed. Nevertheless, we tested the effect of 50 µm microrollers on the cells. We cultured 10^4 human umbilical vein endothelial cells (HUVECs) on 0.32 cm^2 area and introduced 308 ± 67 microrollers of 50 µm on top of the cells. Then we actuated the microrollers with 80 Hz for 5 min, and then left the microrollers on the cells for 24 h. After 24 h, we performed a viability test and observed that there were no significant differences between the control group, further proving microrollers had no detrimental effect on cells (Figure S6, Supporting Information).

3. Discussion

In this study, we demonstrated how the microtopography effect became much less significant for spherical surface microrollers after a certain size regime in CFD simulations and then presented supporting experimental demonstrations. Our previous work has demonstrated that the microtopography effect was significant for 8 µm spherical microrollers, and created a significant locomotion barrier, especially in physiologically

© 2023 The Authors. Small published by Wiley-VCH GmbH

16136829, 2023, 47, Downloaded from https://onlinelibrary.wiley.com/doi/10.1002/smll.202303396 by Turkey Cochrane Evidence Aid, Wiley Online Library on [30/02/2025]. See the Terms and Conditions (https://onlinelibrary.wiley.com/terms-and-conditions) on Wiley Online Library for rules of use; OA articles are governed by the applicable Creative Commons License

relevant flows.[6a] However, anisotropic-shaped microrollers in the same size regime have rendered hydrodynamic interactions with the microtopographies safer and overcame the microtopography effect.[6a] Here, we showed that the microtopography effect could also be tackled by using bigger spherical microrollers of which the fabrication was much more effective and easier than the anisotropic microrollers. The fabrication of anisotropic microrollers was low throughput and not deterministic but rather probabilistic, which created an additional limitation to their use for further biomedical applications. On the other hand, using bigger microrollers can cause complications in certain regions of the body, such as occlusions in blood vessels. Therefore, the application windows of the microrollers must be carefully examined for their specific use. For example, such big microrollers can be used to fill the aneurysms in veins or arteries,[21] or possibly other sites of the body.

Medical microrobots, in general, can be utilized in the cavities of the human body, such as blood vessels, the stomach, and the intestine, where the surfaces are covered with biological cells. Blood vessels are arguably the most challenging environment for the navigation of microrobots due to the rheological properties of blood[22] and strong fluidic flows.[1b] Surface microrollers were shown to be effective microrobotic systems to perform upstream locomotion in physiologically relevant flows found in blood vessels.[4b,6a,7a-c,23] However, the force generated by the microrollers decreased by the presence of the microtopographies in static conditions (Figures 1–4), and the extent of the force decreases would be even higher in the presence of physiologically relevant flows. Therefore, the force decreases caused by the microtopographies must be minimal for safer locomotion against physiological flows, which was possible with bigger spherical microrollers shown here. On the other hand, the locomotion of bigger microrollers would be challenging in smaller vessels due to serious confinement effects.[6b]

The experimental characterizations with surface microrollers can be extended with 3D printed synthetic microtopographies for more systematic comparison as in our previous study[6a]; however, the in vitro microtopographies (Figure 6) also provided a robust platform for brief testing of microrobots. The chicken embryo models can present a convenient platform for the test of microrobots since the blood vessels can be observed with a light microscope. Therefore, any microrobotic system can be tested with such a platform for real-life applications. However, the beforementioned issues must be resolved to perform systematic experiments with such a platform. In addition, the CFD simulations in this study consider rigid-solid boundaries and do not account for material elasticity. Including additional physics in the current simulations would substantially increase the computational cost, rendering the study infeasible with such a high number of cases. However, given the magnitude of forces generated by the microrollers, the topographies' rigidity and stiffness were anticipated to have negligible impact in our case. Synthetic or biological experiments extensively supported the CFD analyses presented in this manuscript, and the results of the CFD analyses align completely with the experimental findings. Significant deformations are anticipated to only occur with much larger microrollers that meet the force requirements.

The other physical limitations on locomotion must be thoroughly studied, such as confinement[6b] or flow effects.[8b] The combination of these effects will introduce additional complexities for locomotion. Therefore, investigating the combined mechanisms is crucial for robust control of microrobots to perform their biomedical task. Surface microrollers, on the other hand, is a relatively well-established and explored platform[4b,6,7] for various biomedical applications. Their locomotion characteristics in different media,[4b,6,7,16] biomedical functions,[7a] biocompatibility, and medical imaging aspect[4b] were relatively well understood. In addition to these, they offer great advantages such as being the fastest magnetic microrobot in its size scale[6a,7a] and their fabrication is scalable and relatively simple. The only drawback of the surface microroller system is that it requires a boundary effect, as rotational motion without a boundary does not result in translational motion.

Microrollers have found medical applications only in cavities of the body, such as blood vessels, procedures as their micron size prevents tissue penetration. These microrollers are envisioned to be used in the treatment of aneurysms[21a,24] and for endovascular drug delivery.[25] These medical interventions require precise placement of microrollers near vessel walls using catheters. For these operations, medical imaging of microrollers is a crucial consideration[5a,e] and more research must be focused in that direction. The real-time imaging possibilities of microrollers must be explored with different imaging modalities to ensure safe interventions.[5c] In the case of aneurysm treatment, microrollers can be actively guided to hard-to-reach bulges in the aneurysm, acting as filling agents to prevent rupture. In drug delivery applications, microrollers can target cancer invasions in blood vessels[26] or cancer-associated endothelial cells[27] through interactions with antibody receptors,[7a] releasing the drug directly into the cancerous tissue. Still, all these applications require fundamental research from medical imaging, locomotion, and biocompatibility aspects.

Overall, we investigated the performance of spherical microrollers with increased sizes on biologically relevant microtopography dimensions. The CFD analyses suggested that the microtopography effect became less significant with increased microroller diameter, while the experimental findings supported the CFD simulations. The rational design principles revealed here provide a better understanding of surface microrollers toward their practical applications in biomedical engineering.

4. Experimental Section

Computational Fluid Dynamics (CFD) Analyses: COMSOL Multiphysics 6.0 Simulation Software (COMSOL, Inc.) was used to simulate microrollers and calculate the forces acting on the microrollers near microtopographies using laminar flow interface physics by solving the Navier–Stokes equations. Previously validated simulations were used with some modifications.[6b] Briefly, two different mesh regions were defined in the simulation environment; the first one was around the microroller, and the second one covered the remaining spaces. $3a \times 3a \times 3a$, where minimum element size, maximum element size, maximum element growth rate, curvature factor, and the resolution of narrow regions were defined in COMSOL as $a/50$, a/5, 1.2, 0.05, and 1.5, respectively, for all sizes, where a is the radius of the microroller. For the second mesh, "extremely fine" built-in mesh settings were used in $40a \times 40a \times 40a$ dimensions. The density and the dynamic viscosity of the fluid were taken as $\rho = 1000$ kg m^{-3} and $\mu = 1$ cP. The boundaries other than microrollers' were defined as no-slip boundaries.

© 2023 The Authors. Small published by Wiley-VCH GmbH

16136829, 2023, 47, Downloaded from https://onlinelibrary.wiley.com/doi/10.1002/smll.202303396 by Turkey Cochrane Evidence Aid, Wiley Online Library on [20/02/2025]. See the Terms and Conditions (https://onlinelibrary.wiley.com/terms-and-conditions) on Wiley Online Library for rules of use; OA articles are governed by the applicable Creative Commons License

Fabrication and Actuation of Surface Microrollers: Previously fabricated and characterized microrollers were used in the previous study.[13] Briefly, Janus microrollers were fabricated by sequentially sputtering Ni and Au nanofilms on a pre-dried monolayer of silica (SiO_2) particles of 4 and 50 µm diameter (Microparticles GmbH, Corpuscular Inc.) using benchtop sputter coating system (Leica EM ACE600, Leica Microsystems). 1000 nm Ni was used for 4 µm 1800 nm was Ni used for 50 µm particles with all microparticles consisting of 50 nm Au as passivating layers. The magnetization direction of the Janus microparticles was oriented toward out of the cap by applying a 1.8 T uniform magnetic field in a vibrating-sample magnetometer (VSM; MicroSense, Lowell, MA). The particles were half-coated enabling safe rolling locomotion on the surfaces. If the particles had a full coating, the total magnetic moment could cancel each other inside, so that rolling locomotion with high frequencies could not be obtained. The microrollers were actuated using a custom-made five-coiled electromagnetic coil system placed on a microscope (Zeiss Axio Observer A1, Carl Zeiss). The microrollers were actuated using uniform rotating magnetic fields with an amplitude of 10 mT that enables surface rolling and steering control for all experimental demonstrations. The synthetic microtopographies were fabricated from IP-S photoresist using a commercially available two-photon lithography system (Photonic Professional, Nanoscribe GmbH) using 63x objective. The 3D microtopographies were created with SolidWorks (Dassault Systèmes).

In Vitro Cell Culture Experiments: In vitro experiments were performed with a previously used and characterized system.[16] The HT-29 cells (ATCC, Rockville, MD, USA) were cultured in Dulbecco's modified Eagle's medium supplemented with 10% (v/v) FBS, penicillin (50 UI mL^{-1}), and streptomycin (50 µg mL^{-1}) in a humidified, 37 °C, 5% CO_2 environment using 75 cm^2 polystyrene cell culture flasks. After, the cells were subcultured to fibronectin-coated and sterilized glass slides and cultured for 3 days to reach confluence. Then, the cells were fixed using 4% paraformaldehyde to keep the topography of the cells intact during magnetic actuation experiments. Human umbilical vein endothelial cells (HUVECs) were obtained from the American Type Culture Collection (ATCC, Rockville, MD, USA). HUVECs were grown in endothelial cell growth basal medium 2 (CC-3156, Lonza) supplemented with endothelial cell growth media 2 SingleQuots (CC-4176, Lonza) in a 5% CO_2, 95% air-humidified atmosphere using 75 cm^2 polystyrene cell culture flasks. 10^4 HUVECs were subcultured into fibronectin-treated glass slides with 0.32 cm^2 area. After reaching ≈80% confluence, 308 ± 67 microrollers were introduced into the HUVECs and locomoted over the cells in a way that they sweep the whole surface area of the glass slides for 5 min at 80 Hz rotation frequency at 10 mT amplitude. After 24 h, the viability of the cells was investigated using LIVE/DEAD Viability/Cytotoxicity Kit (Invitrogen, Thermo Fisher Scientific, Waltham, MA) compared to the control group. The data was collected from three samples from each group.

Preparation of Chicken Embryo Vascular Model: Fertilized White Leghorn chicken eggs (SPF Eggs, VALO BioMedia, Osterholz-Scharmbeck, Germany) were placed in a commercial incubator (Pro PX 20, RCOM Incubators, KS, USA) and were frequently turned to prevent the embryo from sticking to its membranes. The incubation period for these eggs was 14 days, at which point the embryos were euthanized. To investigate the development of the circulatory system, chick embryos were selected from the range of 7 to 14 days of incubation, which corresponds to stages 32–40 according to the Hamburger and Hamilton scale.[28] After experiments, the chick embryos were euthanized by decapitation.

For intravascular injection, the eggs were examined using the candling method to locate the air cell. Then, a scalpel and tweezers were used to carefully open the eggshell above the chorioallantoic membrane (CAM), which is the embryonic membrane that surrounds the developing chick. The egg was then placed in a holder under a microscope to view the outer shell membrane. To make the blood vessels of the CAM visible, the outer shell membrane was moistened with a PBS solution. The outer shell membrane was removed without damaging the CAM vessels, and a chorioallantoic vein of similar diameter was identified by its bright red color and the direction of erythrocyte flow. Microrollers with a diameter of 50 µm were injected into the umbilical vein using a 30-gauge needle.[17]

Supporting Information

Supporting Information is available from the Wiley Online Library or from the author.

Acknowledgements

This work was funded by the Max-Planck-Gesellschaft.
Open access funding enabled and organized by Projekt DEAL.

Conflict of Interest

The authors declare no conflict of interest.

Data Availability Statement

The data that support the findings of this study are available from the corresponding author upon reasonable request.

Keywords

computational fluid dynamics, hydrodynamics, lab-on-a-chip, medical microrobots, microrobotics, surface microrollers

Received: April 22, 2023
Revised: July 10, 2023
Published online: July 24, 2023

[1] a) M. Sitti, *Mobile Microrobotics*, MIT Press, Cambridge, MA **2017**; b) B. J. Nelson, I. K. Kaliakatsos, J. J. Abbott, *Annu. Rev. Biomed. Eng.* **2010**, *12*, 55.
[2] J. Jiang, Z. Yang, A. Ferreira, L. Zhang, *Adv. Intell. Syst.* **2022**, *4*, 2100279.
[3] D. Liu, T. Wang, Y. Lu, *Adv. Healthcare Mater.* **2022**, *11*, 2102253.
[4] a) S. Wang, X. Liu, Y. Wang, D. Xu, C. Liang, J. Guo, X. Ma, *Nanoscale* **2019**, *11*, 14099; b) U. Bozuyuk, E. Suadiye, A. Aghakhani, N. O. Dogan, J. Lazovic, M. E. Tiryaki, M. Schneider, A. C. Karacakol, S. O. Demir, G. Richter, M. Sitti, *Adv. Funct. Mater.* **2022**, *32*, 2109741.
[5] a) A. Aziz, S. Pane, V. Iacovacci, N. Koukourakis, J. Czarske, A. Menciassi, M. Medina-Sánchez, O. G. Schmidt, *ACS Nano* **2020**, *14*, 10865; b) M. Medina-Sánchez, O. G. Schmidt, *Nature* **2017**, *545*, 406; c) P. Wrede, O. Degtyaruk, S. K. Kalva, X. L. Deán-Ben, U. Bozuyuk, A. Aghakhani, B. Akolpoglu, M. Sitti, D. Razansky, *Sci. Adv.* **2022**, *8*, eabm9132; d) Z. Wu, L. Li, Y. Yang, P. Hu, Y. Li, S.-Y. Yang, L. V. Wang, W. Gao, *Sci. Rob.* **2019**, *4*, eaax0613; e) A. Aziz, J. Holthof, S. Meyer, O. G. Schmidt, M. Medina-Sánchez, *Adv. Healthcare Mater.* **2021**, *10*, 2101077.
[6] a) U. Bozuyuk, Y. Alapan, A. Aghakhani, M. Yunusa, M. Sitti, *Proc. Natl. Acad. Sci. USA* **2021**, *118*, e2022090118; b) U. Bozuyuk, A. Aghakhani, Y. Alapan, M. Yunusa, P. Wrede, M. Sitti, *Nat. Commun.* **2022**, *13*, 6289.
[7] a) Y. Alapan, U. Bozuyuk, P. Erkoc, A. C. Karacakol, M. Sitti, *Sci. Rob.* **2020**, *5*, eaba5726; b) X. Qi, S. Wang, S. Ma, K. Han, X. Bian, X. Li, *Phys. Fluids* **2021**, *33*, 121908; c) Z. Wu, Y. Zhang, N. Ai, H. Chen, W. Ge, Q. Xu, *Adv. Intell. Syst.* **2022**, *4*, 2100266; d) L. Wang, H. Gao, H. Sun, Y. Ji, L. Song, L. Jia, C. Wang, C. Li, D. Zhang, Y. Xu, H. Chen, L. Feng, *Research 2023*, *6*, 0088.
[8] a) G. Yan, B. Xu, X. Shi, Y. Zong, Y. Wu, J. Liu, Y. Ouyang, G. Chen, J. Cui, Y. Mei, *Appl. Mater. Today* **2022**, *27*, 101457; b) U. Bozuyuk,

© 2023 The Authors. Small published by Wiley-VCH GmbH

16136829, 2023, 47, Downloaded from https://onlinelibrary.wiley.com/doi/10.1002/smll.202303396 by Turkey Cochrane Evidence Aid, Wiley Online Library on [30/02/2025]. See the Terms and Conditions (https://onlinelibrary.wiley.com/terms-and-conditions) on Wiley Online Library for rules of use; OA articles are governed by the applicable Creative Commons License

H. Ozturk, M. Sitti, *Adv. Intell. Syst.* **2023**, *18*, 2300099; c) E. B. van der Wee, B. C. Blackwell, F. Balboa Usabiaga, A. Sokolov, I. T. Katz, B. Delmotte, M. M. Driscoll, *Sci. Adv.* **2023**, *9*, eade0320.

[9] a) P. F. Davies, T. Mundel, K. A. Barbee, *J. Biomech.* **1995**, *28*, 1553; b) M. Sato, K. Nagayama, N. Kataoka, M. Sasaki, K. Hane, *J. Biomech.* **2000**, *33*, 127.

[10] S. Neelam, P. R. Hayes, Q. Zhang, R. B. Dickinson, T. P. Lele, *Sci. Rep.* **2016**, *6*, 19689.

[11] A. J. Goldman, R. G. Cox, H. Brenner, *Chem. Eng. Sci.* **1967**, *22*, 637.

[12] D. Disharoon, K. B. Neeves, D. W. M. Marr, *Langmuir* **2019**, *35*, 3455.

[13] U. Bozuyuk, H. Ozturk, M. Sitti, *Sci. Rep.* **2023**, *13*, 10196.

[14] H. Jaganathan, B. Godin, *Adv. Drug Delivery Rev.* **2012**, *64*, 1800.

[15] E. Denkhaus, K. Salnikow, *Crit. Rev. Oncol. Hematol.* **2002**, *42*, 35.

[16] A. Aghakhani, A. Pena-Francesch, U. Bozuyuk, H. Cetin, P. Wrede, M. Sitti, *Sci. Adv.* **2022**, *8*, eabm5126.

[17] T. L. M. Mulder, J. C. van Golde, F. W. Prinzen, C. E. Blanco, *Cardiovasc. Res.* **1997**, *34*, 525.

[18] K. Jin, J. Zhou, G. Wu, Z. Lian, Z. Zhao, S. Zhou, C. Chen, H. Sun, Y. Niu, Q. Zuo, Y. Zhang, J. Song, G. Chen, B. Li, *J. Vis. Exp.* **2022**, *184*, e63458.

[19] M. Sarmadi, A. M. Behrens, K. J. McHugh, H. T. M. Contreras, Z. L. Tochka, X. Lu, R. Langer, A. Jaklenec, *Sci. Adv.* **2020**, *6*, eabb6594.

[20] D. Gonzalez-Rodriguez, L. Guillou, F. Cornat, J. Lafaurie-Janvore, A. Babataheri, E. de Langre, A. I. Barakat, J. Husson, *Biophys. J.* **2016**, *111*, 2711.

[21] a) A. C. Bakenecker, A. von Gladiss, H. Schwenke, A. Behrends, T. Friedrich, K. Lüdtke-Buzug, A. Neumann, J. Barkhausen, F. Wegner, T. M. Buzug, *Sci. Rep.* **2021**, *11*, 14082; b) J. Oechtering, P. J. Kirkpatrick, A. G. K. Ludolph, F. J. Hans, B. Sellhaus, A. Spiegelberg, T. Krings, *Neurosurgery* **2011**, *68*, 1388.

[22] E. Nader, S. Skinner, M. Romana, R. Fort, N. Lemonne, N. Guillot, A. Gauthier, S. Antoine-Jonville, C. Renoux, M.-D. Hardy-Dessources, E. Stauffer, P. Joly, Y. Bertrand, P. Connes, *Front. Physiol.* **2019**, *10*, 1329.

[23] a) C. J. Zimmermann, P. S. Herson, K. B. Neeves, D. W. M. Marr, *Sci. Rep.* **2022**, *12*, 5078; b) Z. Zhang, A. Sukhov, J. Harting, P. Malgaretti, D. Ahmed, *Nat. Commun.* **2022**, *13*, 7347.

[24] a) D. Jin, Q. Wang, K. F. Chan, N. Xia, H. Yang, Q. Wang, S. C. H. Yu, L. Zhang, *Sci. Adv.* **2023**, *9*, eadf9278; b) J. Oechtering, P. J. Kirkpatrick, A. G. Ludolph, F. J. Hans, B. Sellhaus, A. Spiegelberg, T. Krings, *Neurosurgery* **2011**, *68*, 1388.

[25] M. B. Fish, A. L. Banka, M. Braunreuther, C. A. Fromen, W. J. Kelley, J. Lee, R. Adili, M. Holinstat, O. Eniola-Adefeso, *Sci. Adv.* **2021**, *7*, eabe0143.

[26] N. C. Buchs, M. Chilcott, P. A. Poletti, L. H. Buhler, P. Morel, *World J. Gastroenterol.* **2010**, *16*, 2788.

[27] A. C. Dudley, *Cold Spring Harbor Perspect. Med.* **2012**, *2*, a006536.

[28] V. Hamburger, H. L. Hamilton, *Dev. dyn.* **1992**, *195*, 231.

© 2023 The Authors. Small published by Wiley-VCH GmbH

16136829, 2023, 47, Downloaded from https://onlinelibrary.wiley.com/doi/10.1002/smll.202303396 by Turkey Cochrane Evidence Aid, Wiley Online Library on [20/02/2025]. See the Terms and Conditions (https://onlinelibrary.wiley.com/terms-and-conditions) on Wiley Online Library for rules of use; OA articles are governed by the applicable Creative Commons License